Title: Highly Efficient Visible Light Catalysts Driven by Ti3+-VO-2Ti4+-N3- Defect Clusters

Authors: Yun Liu; Qingbo Sun; Shaoyang Zhang; David Cortie; Julien Langley; Nicholas Cox; Terry J. Frankcombe; Jie Gao; Hua Chen; Ray L. Withers; Felipe Kremer; Dehong Yu; Frank Brink; Wensheng Shi

To be cited as: ChemNanoMat 10.1002/cnma.201800400

Link to VoR: https://doi.org/10.1002/cnma.201800400

Highly Efficient Visible Light Catalysts Driven by Ti^{3+}-V_O-$2Ti^{4+}$-N^{3-} Defect Clusters

Qingbo Sun,[a] Shaoyang Zhang,[b] David Cortie,[a,c] Julien Langley,[a] Nicholas Cox,[a] Terry J. Frankcombe,[d] Jie Gao,[e] Hua Chen,[f] Ray L. Withers,[a] Felipe Kremer,[f] Dehong Yu,[c] Frank Brink,[f] Wensheng Shi,[b] and Yun Liu*[a]

Abstract: Local defect structures play significant roles on material properties, but they are seriously neglected in the design, synthesis, and development of highly efficient TiO_2-based visible light catalysts (VLCs). Here, we take anatase TiO_2 nanocrystals that contain (Ti^{3+}, N^{3-}) ions and have the complicated chemical formula of $(Ti^{4+}_{1-x}Ti^{3+}_x)(O^{2-}_{2-y-z}N^{3-}_y\square_z)$ as an example, and point out that the formation of Ti^{3+}-V_O-$2Ti^{4+}$-N^{3-} local defect clusters is a key missing step for significantly enhancing VLC properties of host TiO_2 nanocrystals. Experimental and theoretical investigations also demonstrate the emergent behaviors of these intentionally introduced defect clusters for developing highly efficient VLCs. This research thus not only provides highly efficient visible light catalysts for various practical applications but also addresses the significance of local defect structures on modifying material properties.

The development of highly efficient visible light catalysts (VLCs) can help to alleviate the serious environmental pollution and overcome the current energy crisis since they can directly harness visible light from the solar spectrum to drive a range of catalytic reactions such as generating hydrogen from water, degrading organic pollutants or removing hazardous chemicals in wastewater and air.[1-5] To develop highly efficient TiO_2-based VLCs, various strategies are attempted to date, for instance, cation/anion mono-doping,[6,7] cation-cation/cation-anion/anion-anion co-doping,[8-10] noble metal element modifying[11,12] as well as multi-compositional mixing.[13,14] The former two chemically incorporate dopants or co-dopants into host TiO_2 crystal structures while the latter two physically add another species on material surfaces. The improved VLC properties are then attributed to either the adjustment of the band structure of materials, or the generation of surface plasma resonance effects, or the introduction of secondary species themselves. Although these strategies represent a substantial progress in the research and development of TiO_2-based VLCs, most of them are only active in a certain solar spectral region or only moderately improve VLC properties.

More recent efforts for achieving highly efficient VLCs have been made on TiO_2 materials that contain N^{3-} or Ti^{3+} ions since it is generally believed that the hybridization of N 2*p* and O 2*p*, or Ti^{4+} 3*d* and Ti^{3+} 3*d* orbitals enables narrowing the bandgap, extending light absorption and thus enhancing VLC efficiency.[6,15-19] However, the results are not consistent. Some researchers reported that the incorporation of N^{3-} or Ti^{3+} ions significantly enhanced VLC efficiency[6,15-17] while others found that they were only slightly effective or even completely ineffective.[18,19] Furthermore, the mechanisms underlying VLC effects are also ambiguous. The formation of isolated states between forbidden bands,[19,20] multiple light reflections from material hierarchical structures,[17] the introduction of oxygen vacancies,[18] the optical intragap absorption,[10] as well as the appearance of a diamagnetic cluster[21] were all suggested as potential mechanisms for those observed photocatalytic phenomena. From a structural perspective, the incorporation of N^{3-} or Ti^{3+} ions will concurrently introduce oxygen vacancies into TiO_2 for charge balance and then inevitably deteriorate photocatalytic performances through forming "recombination centers" to trap photo-excited carriers. To achieve higher VLC performances, special material structural designs, for example, lattice-disorder engineering of nanocrystalline surfaces,[15] deliberately surficial doping,[17] passivated co-doping,[22] and compositional gradient distribution of dopant ions[9] are normally further required and thus lead to a technological difficulty in their controllable preparation.

[a] Research School of Chemistry, The Australian National University, Canberra, Australian Capital Territory, 2601, Australia.
[b] Technical Institute of Physics and Chemistry, Chinese Academy of Sciences, Beijing, 100190, China.
[c] The Australian Nuclear Science and Technology Organisation, Lucas Height, New South Wales, 2234, Australia.
[d] School of Physical, Environmental and Mathematical Sciences, University of New South Wales, Canberra, Australian Capital Territory, 2601, Australia.
[e] Analysis and Testing Centre for Inorganic Materials, Shanghai Institute of Ceramics, Chinese Academy of Sciences, Shanghai, 200050, China.
[f] Centre for Advanced Microscopy. The Australian National University, Canberra, Australian Capital Territory, 2601, Australia.
Supporting information for this article is given via a link at the end of the document.

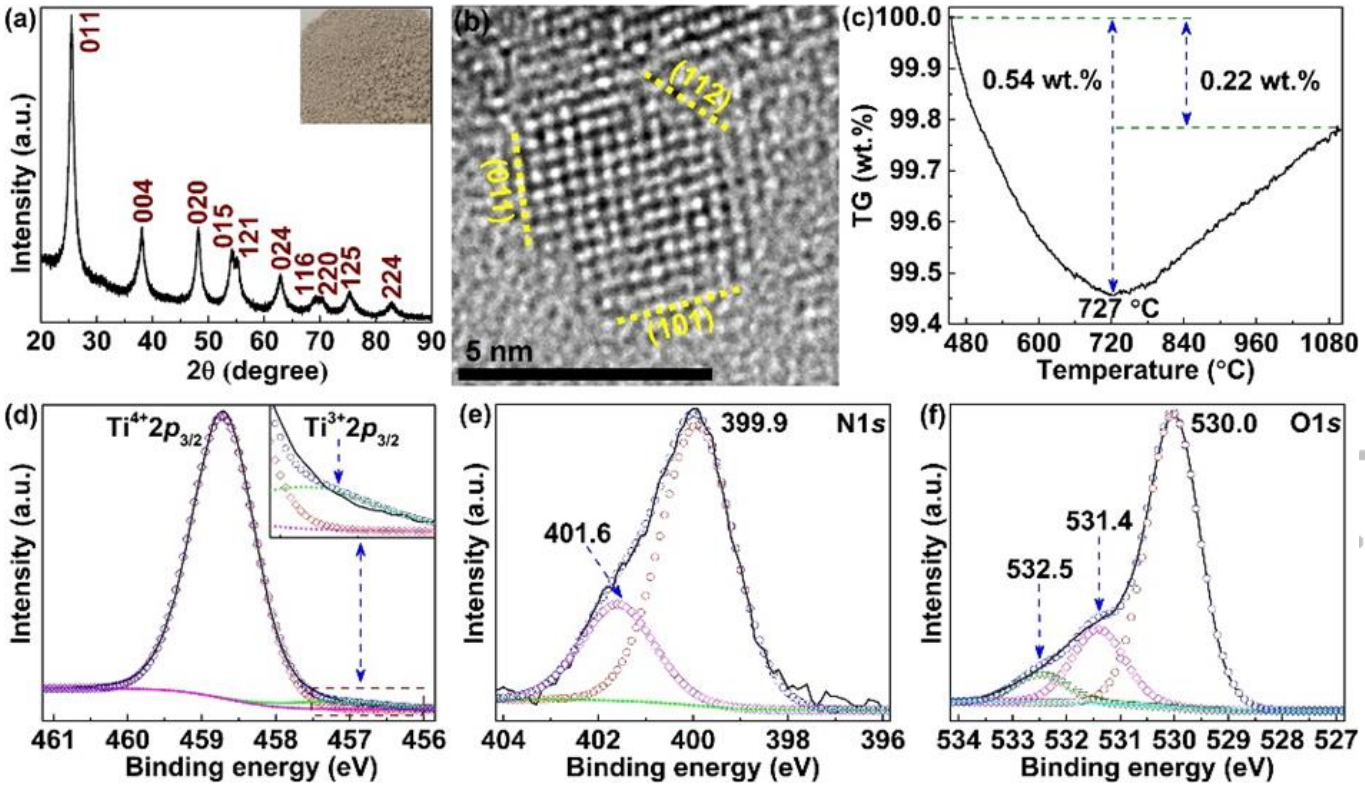

Figure 1. XRD pattern (a), HRTEM lattice image (b), TGA curve (c), and XPS data (d-f) of the $(Ti^{4+}_{0.9619}Ti^{3+}_{0.0381})(O^{2-}_{1.9352}N^{3-}_{0.0305}\square_{0.0343})$ nanocrystals. The inset of (a) is their optical photograph.

Simultaneous incorporation of Ti^{3+} and N^{3-} ions into TiO_2 is an effective and promising way to prepare novel TiO_2-based VLCs. This is because (1) additional cationic dopants are not involved in contrast to other (cation, N^{3-}) co-doping methods; (2) N^{3-} doping levels may be increased significantly by generating some synergistic effects with Ti^{3+} ions; (3) special material structural designs are not required to effectively separate photo-generated charge carriers; and (4) VLC performances of resultant materials can be enhanced exponentially compared to their respective cases. Although the simultaneous introduction of Ti^{3+} and N^{3-} into TiO_2 has so many potential advantages, its chemical synthesis is still technologically difficult. Hydrogenation and nitridation co-treatment of rutile TiO_2 nanowire arrays,[23] calcination and subsequent vacuum activation of amorphous precipitates pre-prepared by a sol-gel technique,[24] and direct solvothermal reaction synthesis using diethylentriamine as a nitrogen source[25] were all attempted. These routes not only need complex experimental processes or long reaction periods but also result in a low N^{3-} doping level (≤ 2at.%), a non-equivalent Ti^{3+}/N^{3-} ratio or an inhomogeneous distribution of Ti^{3+} and N^{3-} ions. This leaves an uncertainty as to whether the improved photocatalytic activity is really determined or dominated by the introduction of Ti^{3+} and N^{3-} ions. Our recent work on the development of highly efficient TiO_2-based VLCs demonstrated the significance of introducing a high but equal concentration of (N^{3-}, Nb^{5+}) defect pairs for outstanding photocatalytic properties.[26,27] This, in combination with our previous research on (In^{3+}, Nb^{5+}), (Al^{3+}, Nb^{5+}), (Mg^{2+}, Ta^{5+}), (Zn^{2+}, Nb^{5+}) and (In^{3+}, Ta^{5+}) co-doped rutile/anatase TiO_2 ceramics/nanocrystals,[28-34] suggests the complexity of ionic co-doping in structurally strongly correlated oxides. The introduced extrinsic ions may stay as isolated point defects in host materials and may also form defect-pairs or clusters coupled with the host ions and local crystal structures. The former presents an additive effect of point defects while the latter leads to significant synergistic behaviors. The defect formation strongly depends on the selection of extrinsic ions, the preparation conditions and the methods used for material synthesis.

Here, we strategically design a new approach to simultaneously incorporate Ti^{3+} and N^{3-} ions into TiO_2 with high and nearly equal concentrations for a real synergistic interaction between the introduced cations and anions. That is, Ti^{3+} and N^{3-} ions are simultaneously introduced into TiO_2 crystal structures under solvothermal reaction conditions using concentrated nitric acid as a nitrogen source, titanium tetrachloride as the initial source of Ti^{4+} and Ti^{3+} ions, and ethanol as solvent. The vigorous chemical reaction of concentrated nitric acid with ethanol not only releases significantly high energy to the reaction system but also yields the high N^{3-} doping levels (Note: due to the vigorous reaction and possible explosion of mixing ethanol and concentrated HNO_3, the used volume of ethanol should be far more than that of concentrated HNO_3, only the latter can be slowly added into the former under magnetically stirring, and a large container like beakers is suggested to use as reaction vessels for adequately releasing possible heat). This route also enables related chemical reactions to occur in a close, high pressure and relatively low temperature environment, directly achieves crystalline TiO_2 materials, and effectively prevents nitrogen loss from unnecessary post-

treatments. The solvothermal products synthesized thereof were then characterized as VLCs for purifying wastewater using Rhodamine B as a model pollutant. Density functional theory (DFT) calculations were performed to understand the observed photocatalytic effects and the related mechanisms arising from the formation of local defect clusters. This research demonstrates the importance of local defect structures on material performances and provides a novel route to design and develop visible light catalysts for highly efficient conversion of solar energy.

The XRD pattern of Figure 1a shows that the synthesized solvothermal products have an anatase phase with space group symmetry $I4_1/amd$. Their diffraction peaks are very broad, suggesting the feature of small particle sizes. The calculated results of the Scherrer equation[28] further demonstrate this small feature of synthesized nanoparticles with an average crystal size of ~7.7 nm (Supporting Information, SI-1), which is reasonably consistent to the estimated results of HRTEM lattice images (Figure 1b and SI-2). From the optical photograph in the insert of Figure 1a, we find that the synthesized nanoparticles are pale yellow. This colour indicates the underlying visible light absorption (as discussed below). From a $\langle 11\bar{1} \rangle$ oriented HRTEM lattice image (Figure 1b), it is found that the exposed crystal faces of synthesized nanocrystals are (011), (101) and (112) facets, respectively. In addition, these nanoparticles have a specific surface area of 122.7 m^2/g in terms of the result of nitrogen absorption and desorption experiment (SI-3).

The TGA curve in Figure 1c shows that the weight of synthesized nanoparticles firstly decreases (~0.54 wt.%) as the temperature increases from 450 to 727 °C and then continuously increases (~0.22 wt.%) in the temperature range of 727 and 1100 °C. Prior to 450 °C, their weight drops significantly (~13.7 wt.%, SI-4). Such a large low temperature weight loss comes from the removal of physically adsorbed water and/or ethanol, chemically bonded hydroxyl and other organic groups, as confirmed by the FT-IR spectroscopy (SI-5). The small weight loss at higher temperatures (450-727°C), however, should be related to the release of chemically doped nitrogen ions since (1) un-doped TiO_2 normally has no or negligible weight variation in this temperature range;[35-38] and (2) organic groups chemically bonded on nanoparticle surfaces generally do not survive at such a high temperature. Meanwhile, a ~0.54 wt.% nitrogen content corresponds to an atomic percentage of ~3.05 at.% (*i.e.* y≈0.0305) and is in reasonable consistency with the measurement result of a Nitrogen/Oxygen determinator (~2.99 at.%). Further XPS analysis also confirms the existence of N^{3-} dopants through their N 1*s* XPS peak (Figure 1e). Above 727 °C, the 0.22 wt.% weight increase can be attributed to the incorporated oxygen ions at the initial lattice sites of oxygen vacancies or the newly formed positions due to nitrogen release. The O 1*s* XPS peak at ~530.3 eV also reflects a lower oxygen content (~1.9352) in contrast to the standard stoichiometric ratio 2 of un-doped TiO_2 (Figure 1f). This is consistent with the TGA results (Figure 1c) and suggests that oxygen vacancies are produced for charge balance (~3.43 at.%, z≈0.0343).

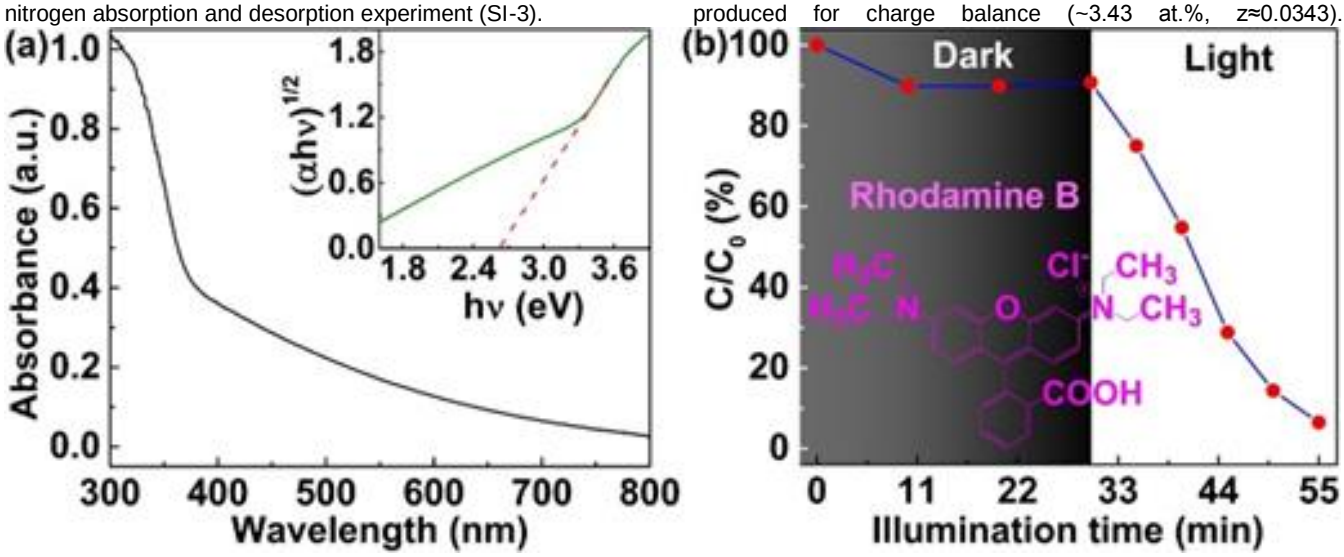

Figure 2. UV-Vis absorption spectrum (a) and associated Tauc plot of the synthesized $(Ti^{4+}_{0.9619}Ti^{3+}_{0.0381})(O^{2-}_{1.9352}N^{3-}_{0.0305}\square_{0.0343})$ nanocrystals. (b) is the photocatalytic degradation of RhB under visible light irradiation (λ≥400 nm) using them as visible light catalysts. Here, "dark" means no light irradiation for achieving an adsorption/desorption equilibrium of RhB on nanoparticle surfaces. "C_0" is the initial RhB solution concentration while "C" indicates the remaining concentration at selected reaction time.

Additionally, we detect the XPS signal of Ti^{3+} ions with a concentration of ~3.81 at.% (x≈0.0381, Figure 1d). The existence of Ti^{3+} ions was further confirmed using EPR spectroscopy (Supporting Information, SI-6). At room temperature, a structureless signal was observed at g = 2.00 of peak-to-peak linewidth 6 mT. Such signals are typically assigned to oxygen species derived from the reaction of Ti^{3+} with O_2 *e.g.* vacancies on the surface of nanoparticles, react with O_2 forming the dominant paramagnetic species observed by other researchers.[39,40] We do not assign here the precise identity of oxygen species. In addition, a weak, axial signal with g-values of 1.98 and 1.95 was also observed at low temperatures, consistent with an anatase that contain Ti^{3+} environment.[39,40] It is thus evident that the bulk nanocrystals have a chemical formula of $(Ti^{4+}_{0.9619}Ti^{3+}_{0.0381})(O^{2-}_{1.9352}N^{3-}_{0.0305}\square_{0.0343})$. The slightly higher N^{3-} doping level achieved here than N^{3-} mono-doping samples should benefit from the synergistic roles of Ti^{3+} ions and the designed solvothermal reaction route.

Figure 2a shows the optical absorption spectra of anatase $(Ti^{4+}_{0.9619}Ti^{3+}_{0.0381})(O^{2-}_{1.9352}N^{3-}_{0.0305}\square_{0.0343})$ nanocrystals. Their light absorption range is very broad and covers the entire visible light regime from 400 nm to 800 nm. Their bandgap calculated through the Tauc plot is ~2.63 eV (the insert of Figure 2a) and becomes narrower than the previously reported TiO_2 nanomaterials that only or simultaneously contain Ti^{3+} and N^{3-} ions.[23-25,41,42] These phenomena demonstrate the significance of introducing highly concentrated Ti^{3+} and N^{3-} ions into TiO_2 crystal structures. Visible light catalytic efficiency is then evaluated by measuring the decomposition rate of RhB and MB, using a 500W Xe lamp with a cutoff wavelength of 400 nm. RhB is one type of potential carcinogen and cannot self-degrade under visible light irradiation (SI-7). It is also difficult to quickly decompose using the commercial P25-TiO_2 photocatalysts (only ~7% at the reaction time of 25 minutes, SI-7 and Table 1). The Anatase $(Ti^{4+}_{0.9619}Ti^{3+}_{0.0381})(O^{2-}_{1.9352}N^{3-}_{0.0305}\square_{0.0343})$ nanocrystals, however, show an excellent visible light catalytic activity (Figure 2b). As seen, it only takes about 25 minutes to accomplish nearly complete decomposition (~94%, Table 1) after an initial adsorption/desorption equilibrium in dark conditions (the adsorption amount of RhB is ~10%, stabilizing within 30 minutes). It indicates that the photocatalytic efficiency of TiO_2 nanocrystals that contain Ti^{3+} and N^{3-} ions is much higher than P25-TiO_2 (Table 1). Further comparing with the experimental results of other TiO_2-based VLCs such as N mono-doped TiO_2,[16] (Bi, Co)/(Fe, Co) co-doped TiO_2,[43] C-TiO_2,[44] g-C_3N_4-TiO_2,[45] Ag_3PO_4-TiO_2,[46] $Zn_xCd_{1-x}S$-

Table 1. The measurement conditions of photocatalytic reaction and the resultant photocatalytic efficiency of anatase TiO_2 nanocrystals that contain Ti^{3+} and N^{3-} ions, commercial Degussa-P25 and other TiO_2-based photocatalysts.

Photocatalysts	Measurement Conditions	VLCs concentration	RhB concentration	VLC efficiency
(Ti^{3+}, N^{3-})-TiO_2 (this work)	Xe lamp (500 W, λ>400 nm)	1 g/L	20 mg/L	~94%@25min
Degussa-P25 (this work)	Xe lamp (500 W, λ>400 nm)	1 g/L	20 mg/L	~7%@25min
N-doped TiO_2[16]	Halogen lamp (1000 W, λ>420 nm)	1 g/L	20 mg/L	~96%@60min
(Bi,Co)-TiO_2[43]	Xe lamp (500 W, λ>400 nm)	1 g/L	20 mg/L	~55%@240min
(Fe,Co)-TiO_2[43]	Xe lamp (500 W, λ>400 nm)	1 g/L	20 mg/L	~64%@240min
C/TiO_2[44]	Xe lamp (500 W, λ>420 nm)	1 g/L	10 mg/L	~96%@60min
g-C_3N_4/TiO_2[45]	Xe lamp (500 W, λ>400 nm)	1 g/L	10 mg/L	~99%@140min
Ag_3PO_4/TiO_2[46]	Xe lamp (500 W, unavailable λ)	1 g/L	10 mg/L	~99%@50min
$Zn_xCd_{1-x}S$/TiO_2[47]	Xe lamp (500 W, λ>420 nm)	1 g/L	10 mg/L	~90%@60min

Note: these experiments were nearly conducted under the similar photocatalytic reaction conditions as ours (*i.e.* using a 500W or more powerful lamp as light sources, loading the same photocatalyst concentration, 1g/L, using rhodamine B as a model pollutant with the concentration of 20mg/L or less).

TiO_2 composites[47] (Table 1), the photocatalytic efficiency of anatase TiO_2 nanocrystals that contain N^{3-} and Ti^{3+} ions is also much higher. When the synthesized nanocrystals were used to decompose another model pollutant-MB, they also showed a high photocatalytic efficiency and ~70% of MB will be decomposed in a short reaction time of 30 minutes. It is thus claimed that the simultaneous introduction of Ti^{3+} and N^{3-} ions is an effective strategy to improve the visible light catalytic activity of host TiO_2 materials.

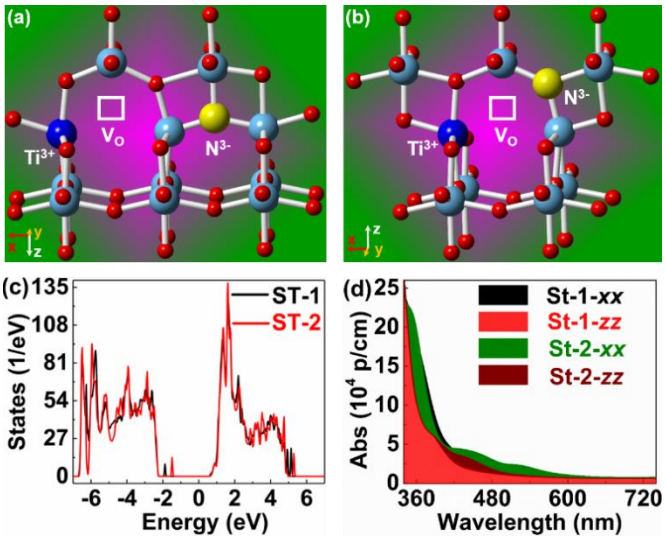

Figure 3, Ball and stick model of two local Ti^{3+}-V_O-$2Ti^{4+}$-N^{3-} clusters formed in anatase TiO_2 crystal structure with lower total energy (a is Structure 1, ST-1 and b is Structure 2, ST-2). (c) is the total density of states of the two different defect structures calculated using the mBJ potential, with E=0 corresponding to the Fermi energy. (d) is the calculated optical absorption coefficient from ST-1 and ST-2 for two components (xx, zz) of the anisotropic optical tensor, showing their light absorption into the entire region (400-700 nm) depicted by the overlaid spectra.

To understand the electronic structure of the synthesized $(Ti^{4+}_{0.9619}Ti^{3+}_{0.0381})(O^{2-}_{1.9352}N^{3-}_{0.0305}\square_{0.0343})$ material or the potential mechanisms of their enhanced VLC performance, DFT calculations were performed using the VASP code in a 3×3×1 supercell. One O^{2-} anion in the anatase TiO_2 crystal structure was substituted by one N^{3-} ion and an additional oxygen vacancy created in various configurations, giving a N^{3-} doping level of 2.78 at.%, which is close to the experimental value of this work (3.05 at.%). Figure 3a shows the lowest energy defect structure among various configurations (structure 1, ST-1). It is composed of one Ti^{3+}, two penta-coordinated Ti^{4+}, one V_O left after the removal of O as well as one N^{3-} binding to one of the two penta-coordinated Ti^{4+} cations. Ti^{3+}-V_O-$2Ti^{4+}$-N^{3-} defect clusters are then formed locally in anatase TiO_2 crystal structure. Structure 2 (ST-2) of Figure 3b also presents the similar defect clusters as ST-1, but its N^{3-} ion just bridges two penta-coordinated Ti^{4+} cations, leading to a ~0.058 eV higher total energy than structure 1. These Ti^{3+}-V_O-$2Ti^{4+}$-N^{3-} defect clusters would avoid the formation of recombination centers in synthesized TiO_2 nanocrystals, and are thus beneficial for highly efficient VLC effects. Other configurations either lie at too high total energy to be present in significant numbers experimentally or do not match the chemical composition of our samples (*e.g.* Ti^{3+} ions cannot be found in the calculation of the scenario of interstitial nitrogen.). Therefore, they are not discussed here. In addition, defect-enhanced charge separation and transfer has been recently observed in protection layer/Si structure of photoanodes.[48] It would be further discussed whether Ti^{3+}-V_O-$2Ti^{4+}$-N^{3-} defect clusters can also separate and transfer photoexcited carriers in our future work.

These two different defect structures significantly modify the electronic structure of TiO_2. Figure 3c exhibits the calculated total density of states (DOS) for ST-1 and ST-2. Their bandgaps are both narrowed to about 2.79 eV in contrast to 2.98 eV of un-doped anatase TiO_2 and are in reasonable accordance with their results of optical absorption measurement (Figure 2a). However, we further find one newly formed mid-gap energy level in the bandgaps. It is shallower in ST-1 and locates ~0.38 eV above the top of valence band, but slightly deeper in ST-2 and locates ~0.75 eV above the top of valence band. The narrowed bandgap and newly introduced mid-gap energy level result in the visible light absorption of $(Ti^{4+}_{0.9619}Ti^{3+}_{0.0381})(O^{2-}_{1.9352}N^{3-}_{0.0305}\square_{0.0343})$ nanocrystals.

In addition, we have calculated the optical absorption coefficient in an attempt to directly observing the enhanced visible light absorption by introducing Ti^{3+}-V_O-$2Ti^{4+}$-N^{3-} defect clusters (Figure 3d). Two absorption tensor components (xx and zz) demonstrate their finite absorption into the visible light regions. Moreover, ST-2 has a stronger visible light absorption ability than ST-1, though the latter is thermodynamically preferred. It is thus clear that the introduction of Ti^{3+}-V_O-$2Ti^{4+}$-N^{3-} defect clusters in anatase TiO_2 host materials is critical to enhance visible light absorption of TiO_2 and is then necessary for outstanding visible light catalytic performances.

In conclusion, Ti^{3+} and N^{3-} ions are successfully incorporated into anatase TiO_2 crystal structure through a novel solvothermal reaction route. These introduced extrinsic ions and associated oxygen vacancies will locally generate Ti^{3+}-V_O-$2Ti^{4+}$-N^{3-} defect clusters for narrowing the bandgap, forming midgap energy level and thus enhancing VLC properties of host TiO_2 materials. The concept, design strategy and synthesis method of highly efficient visible light catalysts driven by defect clusters will provide a guidance for the further development of other photocatalytic materials and also brings new insights for the significance of local defect structures on modifying material properties.

Experimental Section

Anatase TiO_2 nanocrystals that contain Ti^{3+} and N^{3-} ions with the complex chemical formula of $(Ti^{4+}_{1-x}Ti^{3+}_{x})(O^{2-}_{2-y-z}N^{3-}_{y}\square_{z})$ were synthesized by a solvothermal method. In details, $TiCl_4$ (0.68 mL) was first added into ethanol (120 mL) solvent to form a transparent solution under magnetically stirring. Concentrated HNO_3 (69%, 4 mL) were then added into the transparent solution in order to effectively introduce a nitrogen source into the reaction solution. After the above mixture was stirred for two hours at room temperature, it was transferred into an autoclave with an inner volume of about 200 mL. The autoclave was sealed and heated at 200 °C for 12 h in an oven. When the autoclave cooled down to room temperature, the solvothermal product synthesized in the reaction solution was separated by a centrifuge (20,000 rpm), washed with ethanol and distilled water for five times, and finally dried at 60 °C for 12

h. The optimal chemical composition is x≈0.0381, y≈0.0305 and z≈0.0343, respectively [*i.e.* $(Ti^{4+}_{0.9619}Ti^{3+}_{0.0381})(O^{2-}_{1.9352}N^{3-}_{0.0305}\square_{0.0343})$]. Note: the volume of ethanol should be far more than that of concentrated HNO_3 and only the latter can be slowly added into the former under magnetically stirring in order to effectively prevent their too vigorous reaction.

Anatase TiO_2 nanocrystals that contain Ti^{3+} and N^{3-} ions synthesized thereof were analysed by X-ray diffractometer (XRD, PANalytical's X-ray diffractometer with Cu*K*α radiation at the voltage of 45 V, the current of 40 mA, the step size of 0.013° as well as the time per step of 300s), high-resolution transmission electron microscope (HRTEM, JEOL-2100F at the acceleration voltage of 200 kV), and UV-Vis-NIR spectrophotometer (Varian, Cary 5G with the average time of 0.1s, the data interval of 1 nm and the scan rate of 600 nm per minute). The chemical valence and atomic percentage of N and Ti in the prepared nanocrystals were carefully analysed by X-ray photoelectron spectroscopy (XPS, Thermo ESCALAB250Xi) and electron paramagnetic resonance spectrometer (EPR, a Bruker ER200D spectrometer). Moreover, a Nitrogen/Oxygen (N/O) determinator (TC-600, LECO in Helium gas with the flowing velocity of 450 mL per minute) was also used to estimate the nitrogen doping levels. The thermogravimetric (TG) data were collected by STA 8000 (PerkinElmer) with a heating rate of 5 °C per minute in the flowing air (20 mL per minute) to understand the stability and doping concentrations of nitrogen in the samples. The specific surface area was measured through the Brunauer-Emmett-Teller (B.E.T.) method with a QuadraSorb SI-MP instrument. Prior to the measurement, the samples were degassed in vacuum at 423 K for 8 hours. The nitrogen adsorption-desorption data were then recorded at a liquid nitrogen temperature (~77 K). In addition, organic groups on the surfaces of synthesized nanocrystals were carefully measured by a Fourier transform infrared spectroscopy (FT-IR, PerkinElmer) after the achieved samples were buried into KBr pellets.

Rhodamine B (RhB) and methylene blue (MB) was chosen as model organic compounds to evaluate the photocatalytic activities of our synthesized nanocrystals. RhB/MB solution (20 mg L^{-1}) was prepared by mixing RhB/MB (20 mg) with distilled water (1 L). Then, TiO_2 photocatalysts that simultaneously contain Ti^{3+} and N^{3-} ions were added into the RhB/MB solution with a mass concentration of 1 g L^{-1}. A 500 W Xe lamp with a 400 nm cut-off filter provided visible light irradiation for photocatalytic measurement. The solution containing RhB/MB and photocatalysts was stirred for 30 minutes in dark to reach RhB/MB adsorption/desorption equilibrium on the surfaces of synthesized anatase TiO_2 nanocrystals, after which the photocatalytic reaction was initiated by illumination (time=0). The decomposition of RhB/MB was characterized by a UV-Vis-NIR spectrometer based on a typical RhB peak at ~552 nm and a typical MB peak at ~664 nm.

Projector-augmented wave (PAW) calculations were performed using the Vienna Ab initio simulation package (VASP) code.[49,50] A plane wave cutoff of 500 eV was used, with PAW potentials[51] that treat 12, 6 and 5 electrons as valence for Ti, O and N, respectively. Hubbard corrections (DFT+U) were applied with effective U parameters of 7.4 eV for Ti d electrons and 5.4 eV for O and N p electrons. All calculations were spin polarised. Oxidation states were identified by examining angular momentum resolved spin densities in spheres centred on the nuclei. Calculations were performed on a 3×3×1 supercell of the anatase crystallographic unit cell (108 atoms). A 2×2×2 Γ-centred k-point grid was used. The lattice was kept fixed at that optimised for pure anatase using the same computational procedure (a=3.8783 Å, c=9.7701 Å). All results are reported for relaxed ionic positions with no constraints. After structural relaxation, the densities of electronic states were calculated using an accurate all-electron method as implemented in the WIEN2K software.[52] Spin polarised calculations were performed to account for the local moment found on certain Ti atoms. The atomic sphere sizes were set to 1.85, 1.69 and 1.59 atomic units (A.U.) for Ti, O and N, respectively. A 5x5x7 Γ-centred k-point grid was used. Owing to the large size of the supercell cell (71 unique atoms), the plane wave basis was constrained to the maximum value within available memory (RKMax=6.1). Convergence tests on smaller systems using RKMax between 6 and 8 indicate that the lower value is reasonable since the gap is accurate to within 0.1 eV. For the final electronic structure, calculations were made using the sophisticated modified-Becke-Johnson (mBJ) potential that allows a parameter-free method to accurately predict experimental bandgaps, which substantially improves on the Kohn-Shan bandgaps predicted by standard DFT methods.[53] The optical absorption coefficient was then calculated using the joint density of states for both the spin-up and spin-down component, weighted by the respective dipole matrix elements.[54] Only inter-band contributions were considered. The absorption coefficient was calculated from the real and imaginary dielectric constant of the Kramers-Kronig transformation.

Acknowledgements

Q. Sun, D. Cortie, T. J. Frankcome, N. Cox and Y. Liu acknowledge the supports of the Australian Research Council in the form of Discovery Projects and the ARC Future Fellowships program. S. Zhang and W. Shi thank the support from CAS (1A1111KYSB20180017, XDB17030000). The authors acknowledge the facilities, the scientific, technical assistance of the Australian microscopy and microanalysis research facility at the Centre of advanced Microscopy (ANU).

Keywords: Defect cluster • TiO_2 • Visible light catalysts • Solvothermal reaction • Doping

Reference

[1] W. Zhang, W. Lai, R. Cao, *Chem. Rev.* **2017**, *117*, 3717-3797.
[2] S. Wan, J. Qi, W. Zhang, W. Wang, S. Zhang, K. Liu, H. Zheng, J. Sun, S. Wang, R. Cao, *Adv. Mater.* **2017**, *29*, 1700286.
[3] J. Qi, W. Zhang, R. Cao, *Adv. Energy Mater.* **2018**, *8*, 1701620.
[4] J. He, Z. Yan, J. Wang, J. Xie, L. Jiang, Y. Shi, F. Yuan, F. Yu, Y. Sun, *Chem. Commun.* **2013**, *49*, 6761-6763.
[5] D. H. Nam, J. Z. Zhang, V. Andrei, N. Kornienko, N. Heidary, A. Wagner, K. Nakanishi, K. P. Sokol, B. Slater, I. Zebger, S. Hofmann, J. C. Fontecilla-Camps, C. B. Park, E. Reisner, *Angew. Chem. Int. Ed.* **2018**, *57*, 10595–10599.
[6] R. Asahi, T. Morikawa, T. Ohwaki, K. Aoki, Y. Taga, *Science* **2001**, *293*, 269-271.
[7] B. Liu, H. M. Chen, C. Liu, S. C. Andrews, C. Hahn, P. Yang, *J. Am. Chem. Soc.* **2013**, *135*, 9995-9998.
[8] H. Kato, A. Kudo, *J. Phys. Chem. B* **2002**, *106*, 5029-5034.
[9] G. Liu, L.-C. Yin, J. Wang, P. Niu, C. Zhen, Y. Xie, H.-M. Chen, *Energy Environ. Sci.* **2012**, *5*, 9603-9610.
[10] R. Asahi, T. Morikawa, H. Irie, T. Ohwaki, *Chem. Rev.* **2014**, *114*, 9824-9852.
[11] S. A. Ansari, M. H. Cho, *Sci. Rep.* **2016**, *6*, 25405.
[12] M. G. Méndez-Medrano, E. Kowalska, A. Lehoux, A. Herissan, B. Ohtani, S. Rau, C. Colbeau-Justin, J. L. Rodríguez-López, H. Remita, *J. Phys. Chem. C* **2016**, *120*, 25010-25022.
[13] Q. Xiang, J. Yu, M. Jaroniec, *J. Am. Chem. Soc.* **2012**, *134*, 6575-6578.

[14] J. S. Lee, K. H. You, C. B. Park, *Adv. Mater.* **2012**, *24*, 1084-1088.
[15] X. Chen, S. S. Mao, *Chem. Rev.* **2007**, *107*, 2891-2959.
[16] Y. Cong, J. Zhang, F. Chen, M. Anpo, *J. Phys. Chem. C* **2007**, *111*, 6976-6982.
[17] R. Ren, Z. Wen, S. Cui, Y. Hou, X. Guo, J. Chen, *Sci. Rep.* **2015**, *5*, 10714-10724.
[18] Y. Nakano, T. Morikawa, T. Ohwaki, Y. Taga, *Appl. Phys. Lett.* **2005**, *86*, 132104.
[19] R. Kumar, S. Govindarajan, R. K. S. K. Janardhana, T. N. Rao, S. V. Joshi, S. Anandan, *ACS Appl. Mater. Interfaces* **2016**, 8, 27642-27653.
[20] M. Liu, X. Qiu, M. Miyauchi, K. Hashimoto, *Chem. Mater.* **2011**, *23*, 5282-5286.
[21] Z. Zhang, X. Wang, J. Long, Q. Gu, Z. Ding, X. Fu, *J. Cataly.* **2010**, *276*, 201-214.
[22] Y. Q. Gai, J. B. Li, S. S. Li, J. B. Xia, S. H. Wei, *Phys. Rev. Lett.* **2009**, *102*, 036402.
[23] S. Hoang, S. P. Berglund, N. T. Hahn, A. J. Bard, C. B. Mullins, *J. Am. Chem. Soc.* **2012**, *134*, 3659-3662.
[24] Y. Zhou, Y. Liu, P. Liu, W. Zhang, M. Xing, J. Zhang, *Appl. Catal. B: Environmental* **2015**, *170*, 66-73.
[25] G. Li, J. Li, G. Li, G. Jiang, *J. Mater. Chem. A* **2015**, *3*, 22073-22080.
[26] Q. Sun, D. Cortie, S. Zhang, T. J. Frankcombe, G. She, J. Gao, L. R. Sheppard, W. Hu, H. Chen, S. Zhuo, D. Chen, R. L. Withers, G. McIntyre, D. Yu, W. Shi, Y. Liu, *Adv. Mater.* **2017**, *29*, 1605123.
[27] Q. Sun, B. R. McBride, Y. Liu, *Res. Rev. Electrochemistry* **2017**, *8*, 106.
[28] Q. Sun, C. Zheng, L. Q. Huston, T. J. Frankcombe, H. Chen, C. Zhou, Z. Fu, R. L. Withers, L. Noren, J. E. Bradby, J. Etheridge, Y. Liu, *J. Phys. Chem. Lett.* **2017**, *8*, 3249-3255.
[29] Q. Sun, L. Q. Huston, T. J. Frankcombe, J. E. Bradby, T. Lu, C. Zhou, Z. Fu, Y. Liu, *Cryst. Growth Des.* **2017***, 17,* 2529-2535.
[30] W. Hu, Y. Liu, R. L. Withers, T. J. Frankcombe, L. Norén, A. Snashall, M. Kitchin, P. Smith, B. Gong, H. Chen, J. Schiemer, F. Brink, J. Wong-Leung, *Nat. Mater.* **2013**, *12*, 821-826.
[31] W. Hu, K. Lau, Y. Liu, R. L. Withers, H. Chen, L. Fu, B. Gong, W. Hutchison, *Chem. Mater.* **2015**, *27*, 4934-4942.
[32] W. Dong, D. Chen, W. Hu, T. J. Frankcombe, H. Chen, C. Zhou, Z. Fu, X. Wei, Z. Xu, Z. Liu, Y. Li, Y. Liu, *Sci. Rep.* **2017**, *7*, 9950.
[33] X. Wei, W. Jie, Z. Yang, F. Zheng, H. Zeng, Y. Liu, J. Hao, *J. Mat. Chem. C* **2015**, *3*, 11005-11010.
[34] W. Dong, W. Hu, T. J. Frankcombe, D. Chen, C. Zhou, Z. Fu, L. Cândido, G. Hai, H. Chen, Y. Li, R. L. Withers, Y. Liu, *J. Mat. Chem. A* **2017**, *5*, 5436-5441.
[35] C. Wang, Q. Li, R.-D. Wang, *Mater. Lett.* **2004**, *58*, 1424-1426.
[36] S. Janitabar-Darzi, A. R. Mahjoub, A. Nilchi, *Physica E: Low-dimensional Systems and Nanostructures* **2009**, *42*, 176-181.
[37] R.-A. Doong, S.-M. Chang, Y.-C. Hunga, I.-L. Kao, *Sep. and Purifi. Technol.* 2007, 58,192-199.
[38] M. H. Habibin, R. Mokhtari*, J. Therm. Anal. Calorim.* **2013**, *112*, 1179-1183.
[39] T. Berger, M. Sterrer, O. Diwald, E. Knözinger, *ChemPhysChem* **2005**, 6, 2104-2112.
[40] C. P. Kumar, N. O. Gopa, T. C. Wang, M.-S. Wong, S. C. Ke, J. *Phys. Chem. B* **2006**, *110*, 5223-5229.
[41] X. Li, P. Liu, Y. Mao, M. Xing, J. Zhang, *Appl. Cataly. B: Environmental* **2015**, *164*, 352-360.
[42] H. Y. Yin, X. L. Wang, L. Wang, Q. L. Na, H. T. Zhao, *J. Alloys and Compoud.* **2015**, *640*, 68-74.
[43] Z. Wang, C. Chen, F. Wu, B. Zou, M. Zhao, J. Wang, C. Feng, *J. Hazard. Mater.* **2009**, *164*, 615-620.
[44] X. Yu, J. Liu, Y. Yu, S. Zuo, B. Li, *Carbon* **2014**, *68*, 718-724.
[45] X. Chen, J. Wei, R. Hou, Y. Liang, Z. Xie, Y. Zhu, X. Zhang, H. Wang, *Appl. Cataly. B: Environmental* **2016**, *188*, 342-350.
[46] P. Wang, Y. Li, Z. Liu, J. Chen, Y. Wu, M. Guo, P. Na, *Ceram. Int.* **2017**, *43*, 11588-11595.
[47] W. Chang, X. Ren, G. Yang, W. Yan, Y. Guo, *S. Afr. J. Chem.* **2015**, *68*, 138-142.
[48] J. Zheng, Y. Lyu, C. Xie, R. Wang, L. Tao, H. Wu, H. Zhou, S. Jiang, S. Wang, *Adv. Mater.* **2018**, *30*, 1801773.
[49] M. Hacene, A. Anciaux-Sedrakian, X. Rozanska, D. Klahr, T. Guignon, P. Fleurat-Lessard, *J. Comput. Chem.* **2012**, *33*, 2581-2589.
[50] M. Hutchinson, M. Widom, *Comput. Phys. Commun.* **2012**, *183*, 1422-1426.
[51] G. Kresse, J. Joubert, *Phys. Rev. B.* **1999**, *59*, 1758.
[52] P. Blaha, K. Schwarz, G. K. H. Madsen, D. Kvasnicka, J. Luitz, Techn. Universität, Wien, AT. **2001**.
[53] F. Tran, P. Blaha, *Phys. Rev. Lett.* **2009**, *102*, 226401.
[54] C. Ambrosch-Draxi, J. O. Sofo, *Comput. Phys. Commun.* **2006**, *175*, 1-14.

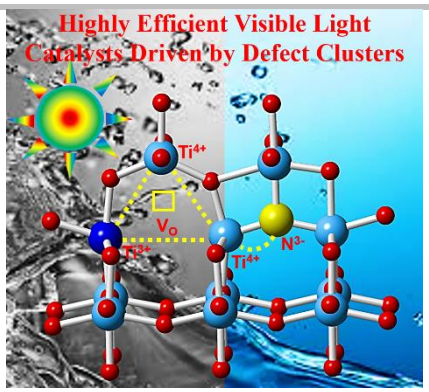

Local defect structure could determine or create novel material properties since it could local chemical environment and subsequently mediate electronic state density of materials. Here, we demonstrate that the deliberate design and formation of Ti^{3+}-V_O-$2Ti^{4+}$-N^{3-} defect clusters in TiO_2 anatase nanocrystals would drive the highly efficient visible light catalytic decomposition of organic contaminates. This research thus not only presents a defect-engineering route to design/develop highly efficient visible light catalysts but also highlights the significance of local defect structures on modifying material properties.